



Remote plasma cleaning of optical surfaces: Cleaning rates of different carbon allotropes as a function of RF powers and distances



M. González Cuxart^a, J. Reyes-Herrera^a, I. Šics^a, A.R. Goñi^{b,c}, H. Moreno Fernandez^a, V. Carlino^d, E. Pellegrin^{a,*}

^a ALBA Synchrotron Light Facility, Carrer de la Llum 2-26, 08290 Cerdanyola del Vallès, Barcelona, Spain

^b Institut de Ciència de Materials de Barcelona (ICMAB-CSIC), Campus UAB, 08193 Bellaterra, Barcelona, Spain

^c ICREA, Passeig Lluís Companys 23, 08010 Barcelona, Spain

^d ibss Group Inc., 111 Anza Blvd., Suite 110, Burlingame, CA 94010, USA

ARTICLE INFO

Article history:

Received 25 May 2015

Received in revised form 9 November 2015

Accepted 12 November 2015

Available online 17 November 2015

ABSTRACT

An extended study on an advanced method for the cleaning of carbon contaminations from large optical surfaces using a remote inductively coupled low-pressure RF plasma source (GV10x DownStream Asher) is reported. Technical and scientific features of this scaled up cleaning process are analysed, such as the cleaning efficiency for different carbon allotropes (amorphous and diamond-like carbon) as a function of feedstock gas, RF power (from 30 to 300 W), and source-object distances (415 to 840 mm). The underlying physical phenomena for these functional dependences are discussed.

© 2015 Elsevier B.V. All rights reserved.

Keywords:

Remote inductively coupled plasma

Plasma cleaning

Graphitic carbon

Diamond-like carbon

Optical emission spectroscopy

X-ray photoemission spectroscopy

Raman spectroscopy

1. Introduction

Previous publications in the field of low-pressure radiofrequency (RF) plasma cleaning of optical surfaces have shown that it is possible to efficiently and safely remove carbon contaminations at the molecular scale [1–7] by using O₂/Ar or H₂/Ar feedstock gas mixtures. In our earlier study [1], the main motivation was to report on a new, safe, and efficient method with well-defined sets of process parameters capable to perform an in-situ cleaning of carbon-contaminated optical elements typically used in UHV chambers, such as synchrotron optics, extreme ultraviolet (EUV) optics, high-power laser optics, etc. In order to achieve this purpose, we performed a comparative work using several different direct capacitive coupled (d-CCP) as well as commercial remote inductively coupled (r-ICP) model GV10x plasma sources at different RF powers.

In this previous publication [1], we worked at 100 W maximum RF power, at close constant distance of about 308 mm between the plasma source and test sample to be cleaned, and in a UHV chamber

of limited dimensions. Maximum carbon cleaning rates of about 12 Å/min could be achieved.

However, UHV chambers where such in-situ cleaning methods will be employed in the field are generally larger than our above test chamber. Thus, moving to a larger UHV chamber was required to approach realistic cleaning conditions of optical components with typical lengths of about 1 m and beyond, including the pertinent source to object dimensions (see Section 2.1 for technical details) while still trying to keep the carbon cleaning rates up. To that end, a more powerful version of the GV10x plasma source has been used (with up to 300 W RF power), which allowed testing the cleaning process at larger source-sample distances and thus to perform a study of cleaning rates as a function of RF plasma power and distances. These data are intended to help develop and optimize more efficient cleaning processes for larger experimental optics setups.

It is also essential to take into account that the real chemical, crystallographic, and morphological structure of carbon contaminations can be rather complex: depending on the specific case, these carbon traces are not only consisting of one single carbon allotrope, but may have an amorphous-like nature, composed of different contributions from sp²- and/or sp³-hybridized carbon species or, in other words, have either a more graphitic or diamond-like nature, etc. Therefore, in this study we also

* Corresponding author. Tel.: +34 935924418; fax: +34 935924301.

E-mail address: epellegrin@cells.es (E. Pellegrin).

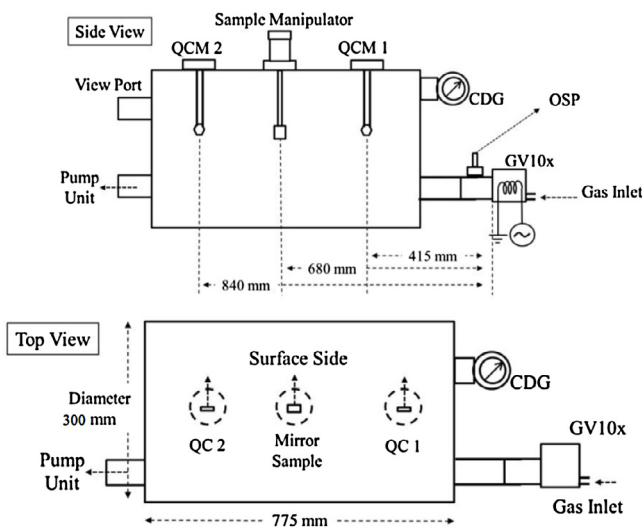


Fig. 1. Conceptual layout of the RF test cleaning chamber (GV10x P3: ICP plasma; OSP: optical spectrometer; QCM: quartz crystal monitor; CDG: capacitive diaphragm).

determined the cleaning rates of amorphous carbon and diamond-like carbon, as a first step towards eventually obtaining a complete library of cleaning rates as a function of the specific carbon chemistry/configuration.

This study is structured as follows: after a concise description of the experimental setup, we present some results from the test sample characterization using x-photoemission spectroscopy (XPS) and Raman spectroscopy. In the next chapter, cleaning rates from the experiments carried out with an O₂/Ar plasma using different RF powers and at two different plasma source-sample distances are given. Following the same scheme, further results from experiments done under H₂/Ar plasma are given. Samples to be cleaned for both studies were amorphous carbon samples (*Amorphous C*). Finally, cleaning rates of diamond-like carbon samples (*DLC*) (as compared to amorphous C samples) using O₂/Ar and H₂/Ar plasma feedstock gases with different RF powers at a fixed source-sample distance will be presented.

Last but not least, we also compare the performance of a 100 W model GV10x P4 plasma source (29 cm³ plasma tube volume) with respect to a 300 W model GV10x P3 plasma source (44 cm³ plasma tube volume). All data shown in this study have been generated using these two plasma sources.

Given the limited geometrical flexibility of our experimental setup, we have not studied any angular dependence with respect to the plasma source axis. However, it should be kept in mind that this additional geometrical parameter will certainly also have an influence on the cleaning rates.

2. Experimental

2.1. Experimental setup

The cleaning experiments were carried out in a horizontal 55 Liter UHV chamber of cylindrical horizontal shape made of 304L (i.e., EN 14301) stainless steel (see the experimental dimensions given in Fig. 1). The GV10x DS Asher Source is installed at one chamber end and the 250 l/s turbo molecular pumping (TMP) unit at the opposite end, so that a constant flux of chemically active species from the upstream plasma source is conducted along the longitudinal axis of the chamber was established (see Fig. 1). Two different GV10x DownStream Asher plasma sources have been used: The P4 source with a smaller plasma tube volume and a

maximum RF power of 100 W as well as the P3 source with a larger plasma tube volume by a factor of 1.5 and a maximum RF power of 300 W. Carbon coated quartz crystals were placed in two quartz crystal microbalances (QCMs) downstream the plasma sources at two different source-sample distances (QCM1: 415 mm, and QCM2: 840 mm). Carbon cleaning rates were calculated from the time evolution of the carbon thickness removed by the plasma as measured by these two QCM balances. Clearly, as this approach makes use of existing technologies for the in-situ determination of quantitative carbon cleaning rates via standard-size small QCM crystals, the cleaning of real-size optical components will have to take into account additional plasma-surface interactions on these real optical components.

The GV10x plasma sources are r-ICP sources that basically consist of a plasma tube and a RF coil coupling the RF power into the plasma tube. The feedstock gas is supplied via the far end of the plasma tube and the exhaust side of the plasma tube is connected to the cleaning chamber via a DN40CF flange (with a roughly 100 mm lateral offset with respect to the chamber cylinder axis). The exhaust end of the plasma tube feeds into the UHV chamber and a downstream plasma of chemically active OI or HI is conducted through the chamber by the differential pressure from the TMP (see Fig. 1 for details on the overall geometry). This warrants for a stable jet of chemically active species from the plasma discharge volume into the downstream cleaning chamber, coherent with the DownStream Asher operation principle of the GV10x source. Further details on the GV10x source can be obtained from the pertinent patents (US Patents 7,015,415, B2; 6,263,831 B1; and 6,112,696).

It should be pointed out that the GV10x DownStream Asher source produces a plasma similar to remote or afterglow plasma. Such a downstream plasma safeguards the objects to be cleaned from the detrimental kinetic effects via a direct exposure to the plasma itself (usually associated with direct DC and RF plasmas), thus restricting the interaction with the surface to be cleaned to chemical processes.

Feedstock gas mixtures were supplied via a custom-made gas supply system with a manual control of mixing rates of the two gases involved and the total pressure inside the chamber. All experiments were done at a total chamber pressure of 0.005 mbar with a feedstock gas flow rate between 2 and 3 sccm.

Optical emission spectra were measured using an Ocean Optics model USB2000+ optical spectrometer via an optical vacuum feedthrough, installed at about 150 mm downstream the exhaust of the GV10x plasma source and perpendicular to the plasma source axis.

Please see reference [1] for further experimental details as well as on the diagnostic tools used in the present study.

2.2. Sample preparation and characterization

Two chemically different types of carbon thin films were deposited on gold-coated QCM crystals were prepared as the test samples to be cleaned. In one case, an amorphous carbon thin film (i.e., a mixture of sp² and sp³ carbon) was deposited onto the QCM crystals by e-beam evaporation from graphitic carbon targets (Goodfellow carbon target model C 009600), carried out in a conventional UHV chamber. Typical amorphous carbon film thicknesses were around 50–200 nm with a thin film diameter of roughly 5 mm. We label and refer to them as *Amorphous C*. Diamond-like carbon sample thin films (i.e., sp³ carbon) were deposited by an arc-discharge method, labelled as *DLC* throughout this study. Typical *DLC* film thicknesses were around 50 nm. Please note that the surfaces of the different carbon-coated QCM crystals (i.e., the *Amorphous C* and *DLC* test samples) were not directly facing the plasma jet from the source using normal incidence but rather via grazing incidence (see Fig. 1, Top View), so that the plasma kinetic effects

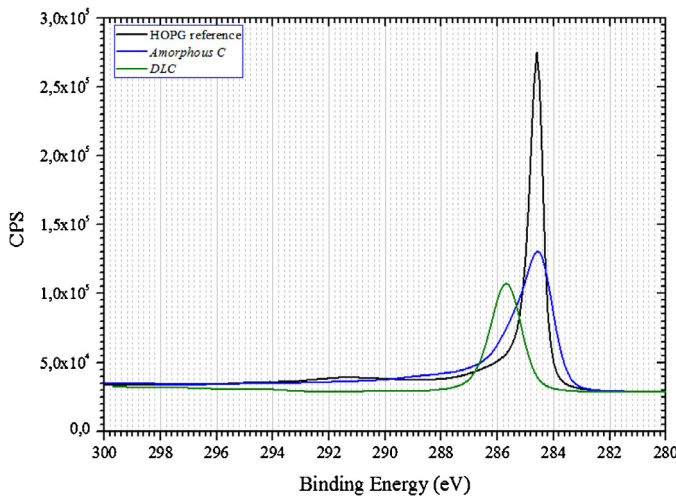


Fig. 2. C1s XPS spectra of the HOPG reference sample and the diamond-like sample (DLC).

– if any – were minimized and thus only chemical effects were effective during the cleaning process.

A comparative C1s XPS analysis of highly oriented pyrolytic graphite (HOPG—as a reference for pure sp^2 C), the amorphous carbon sample (Amorphous C), and the DLC sample (as a reference for sp^3 C) are shown in Fig. 2. The C1s XPS peak for DLC sample is up-shifted by 1.1 eV higher binding energies (BEs) with respect to the C1s line for the HOPG reference sample (284.6 eV), and is thus observed at 285.7 eV BE. This chemical shift gives clear evidence for the sp^3 configuration of the DLC sample [8]. On the other hand, the C1s line from Amorphous C thin films exhibits a broad line shape that is composed of both the C1s lines for sp^2 as well as sp^3 C, thus giving additional spectroscopic evidence (combined with the Raman results given below) for the Amorphous C character of that custom-made carbon thin film sample.

All samples were also characterized by Raman spectroscopy (see Fig. 3(b)). The prominent G line (1583 cm^{-1}) of the HOPG reference sample corresponds to a high-frequency LO phonon within the graphitic planes (E_{2g} phonon in Fig. 3(a)), and it is present in various graphitic structures [9]. Another common peak in graphitic structures is the D peak or defect peak (1345 cm^{-1} ; neither shown nor present in HOPG), which corresponds to a TO phonon around the K point and arises from the breathing modes of six-atom carbon rings (see Fig. 3(a)). The reason why we do not observe the latter in the HOPG reference Raman spectrum is due to the fact that this peak is activated by breakdown of translational invariance due to elastic scattering at crystalline defects or boundaries. Such processes are not possible in a defect-less graphitic lattice (i.e., in HOPG), hence the D peak does not become Raman active in perfectly crystalline samples [10]. Nevertheless, we do observe a very wide peak for the Amorphous C sample (blue solid line), centred just below 1500 cm^{-1} , which is likely the result of a convolution of broadened D and G peaks. The broadening effect that the D and G peaks undergo is due to the small cluster sizes and a further broadening due to inequivalent chemical bonding. The 2D peak (2690 cm^{-1}) corresponds to the D peak overtone (i.e., second order Raman process) and, as it originates from a process where momentum conservation is satisfied by two phonons with opposite wave vectors (double-resonance), no defects are required for its activation, and it is thus always present in sp^2 carbon [11,12].

The “Diamond” peak (at 1332 cm^{-1}) in the diamond single crystal sample corresponds to the first-order Raman scattering mode of diamond [13] and is assigned to the T_{2g} zone centre mode of the

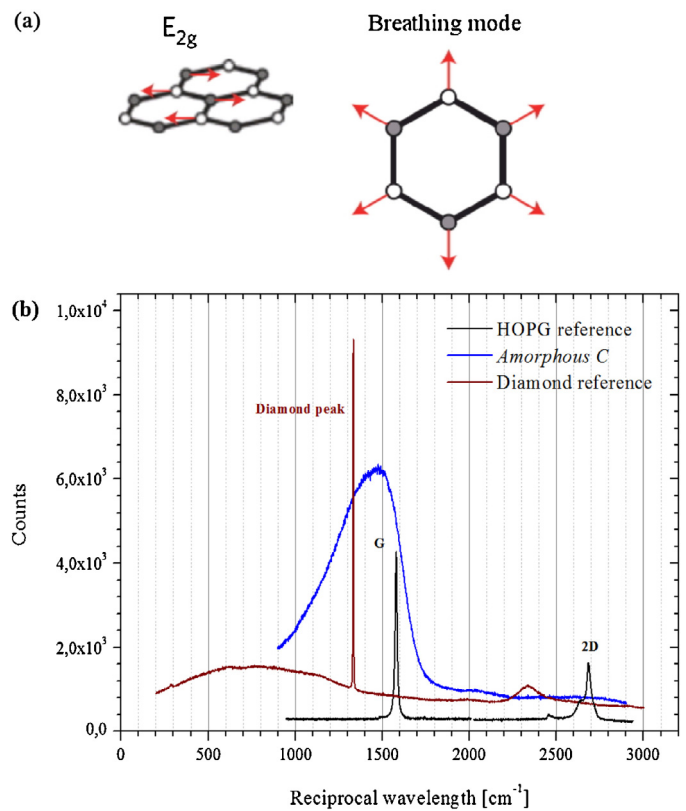


Fig. 3. (a) Raman active phonon displacement pattern in graphitic planes. Empty and filled circles represent inequivalent carbon atoms. E_{2g} give rise to the G peak whereas D peak partly arises from the “Breathing mode”. (b) Raman spectra of the amorphous (Amorphous C) sample, a single-crystalline diamond reference sample, and a HOPG reference samples.

cubic diamond phase. At first glance, this peak does not show up in the Amorphous C case. However, the broad band observed between 1000 and 1700 cm^{-1} (blue solid line in Fig. 3(b))

for the Amorphous C sample is composed of contributions from the widened D and G peaks of sp^2 -coordinated carbon atoms as well as strongly broadened sp^3 “Diamond”-like peaks. Altogether, it corroborates a non-crystalline ordering among the sp^2 and sp^3 -coordinated carbon atoms (i.e., a strong dominance of the amorphous phase).

2.3. Plasma feedstock gas mixtures

Oxygen/argon and hydrogen/argon gas mixtures were used as feedstock gases for the plasma during the cleaning experiments, with a total pressure of 0.005 mbar and an estimated total feedstock gas flow rate between 2 and 3 sccm. These parameters were derived from the optimized concentrations and pressures (i.e., for highest cleaning rates) as found in our previous studies [1]: 95%/5% and 7%/93% for O₂/Ar and H₂/Ar, respectively. Relative concentrations were measured and systematically adjusted (within the practical limits of a manual adjustment) using the corresponding lines in the optical emission spectra (OES) from the plasma as a reference. For the case of the O₂/Ar plasma, we focused onto the atomic lines for the neutral OI (or O⁺) radicals and the neutral ArI atoms, corresponding to the atomic transitions $3s^5S^0$ – $3p^5P$ and $4s^2[1/2]$ – $4p^2[1/2]$, with a line strength of $3.69 \times 10^7\text{ s}^{-1}$ and $4.45 \times 10^7\text{ s}^{-1}$, respectively. In the case of H₂/Ar, we used the neutral HI (or H⁺) radicals ($4.41 \times 10^7\text{ s}^{-1}$) and the same line for ArI [14]. Table 1 gives a summary on the optical transitions used in the present study.

Table 1

Characteristics of specific transitions from optical emission spectra as used in this work.

Radical species	Wavelength [nm]	Lower level Conf., Term, J	Upper level Conf., Term, J	Emission transition probability [s^{-1}]
Ar I (Ar^*)	750.4	$3s^2 3p^5(^2P_{1/2}) 4s, ^2[1/2]^o, 1$	$3s^2 3p^5(^2P_{1/2}) 4p ^2[1/2], 0$	4.45×10^7
O I (O^*)	777.2	$2s^2 2p^3(^4S^*) 3s, ^5S^*, 2$	$2s^2 2p^3(^4S^*) 3p, ^5P, 3$	3.69×10^7
H I (H^*)	656.3	2	3	4.4×10^7

3. Results

3.1. Cleaning experiments using O_2/Ar plasma

We first discuss the cleaning experiments performed on the *Amorphous C* samples using an O_2/Ar plasma. Here, we will focus on the atomic lines for the neutral OI radicals and the neutral ArI atoms. The measured OES spectra from the O_2/Ar experiments for each RF power are shown in Fig. 4(a). Please note the different vertical scales regarding the OES line intensities for each panel that show an increase of the OES lines concomitant with the increasing RF power. As can be seen from Fig. 4(b) for the data from the P3 source, the intensity of the OI lines at 777.2 nm and 844.64 nm increase linearly as a function of RF power, indicating an increase of the density of OI species with RF power. The OES line related to the ArI emission at 750.39 nm remains at almost constant intensity for the whole range of RF power. OI line OES data from the smaller P4 source have been added for reference. On the right hand side axis of Fig. 4(b), we show the oxygen concentration as a function of RF power as derived from an evaluation of the above OES line intensities. This shows a small variation (between 92% and 97%) within the limits of the manual adjustment of the O_2/Ar gas mixture, which is actually much smaller than the increase of the OI line intensity by a factor of about 3.6 when going from 60 to 300 W.

Fig. 5(a) shows the decrease of the carbon layer thickness on both QCM sensors as a function of time and RF power as an additional parameter. As expected and as can be seen from the cleaning rates in Fig. 5(b) derived from Fig. 5(a), we measured faster cleaning rates for the QCM sensor closer to the plasma source (QCM1) as compared to the more distant sample on QCM2, so the quartz crystals on QCM1 became fully cleaned in a shorter amount of time. In the present case, the cleaning rates for both QCM sensors exhibit a linear dependence from the applied RF power which correlates with the linear increase of the OI OES lines in Fig. 4(b). Data using both P3 and P4 plasma sources were acquired for our present case of O_2/Ar plasma cleaning of *Amorphous C* samples (as reported in Section 2.1, the P3 and P4 sources can reach 300 W and 100 W of RF power, respectively, and P3 has a larger plasma cavity volume with respect to that of the P4 by a factor of 1.5).

The results from the linear fits for the data from each individual QCM sensor in Fig. 5(b), for the case of the P3 source, are as follows:

$$C_R[\text{\AA} / \text{min}] = 0.107 \pm 0.010[\text{\AA} / \text{min W}]P_{RF} \quad (1)$$

for QCM1

$$C_R[\text{\AA} / \text{min}] = 0.081 \pm 0.006[\text{\AA} / \text{min W}]P_{RF} \quad (2)$$

for QCM2

where, C_R is the cleaning rate and P_{RF} is the RF power. According to this, the cleaning rates decrease by a factor of roughly 1.3 with an increase in distance by roughly a factor of 2 (i.e., when going from 415 mm for QCM1 to 840 mm for QCM2).

In order to compare the performance of the P4 and P3 plasma sources with different plasma chamber volumes, we included the cleaning rates from a P4 plasma source with a plasma tube being smaller by a factor of 1.5 into Fig. 5(b), while using otherwise

identical experimental setups and parameters. The results from the linear fits for the data from each individual QCM sensor in the case of the P4 source in Fig. 5(b) are as follows:

$$C_R[\text{\AA} / \text{min}] = 0.050 \pm 0.007[\text{\AA} / \text{min W}]P_{RF} \quad (3)$$

for QCM1

$$C_R[\text{\AA} / \text{min}] = 0.018 \pm 0.004[\text{\AA} / \text{min W}]P_{RF} \quad (4)$$

for QCM2

Thus, by increasing the upstream plasma chamber volume by a factor of 1.5, we observe an increase in cleaning rate by a factor of 2.1 and 4.5 for QCM1 (closer to the plasma source) and QCM2 (more distant from the plasma source), respectively. We attribute the increase of cleaning rate to the higher density of chemically active OI (or O^*) species due to the larger plasma tube volume of the P3 plasma source. As can be seen from the comparison between the OES data for the OI line for the P3 and the P4 source in Fig. 4(b), the above difference in cleaning rate is reflected by the difference in the corresponding OI line intensities that increase by roughly a factor of 1.5 when going from the P4 to the P3 source. This corroborates above the assumption that the increase in cleaning rate is due to an increase of chemically active OI (or O^*) species, resulting from the larger plasma tube and thus plasma volume of the P3 source.

3.2. Cleaning experiments using H_2/Ar plasma

We proceed as in the same manner as in the previous case for the cleaning experiments under H_2/Ar plasma. The measured OES spectra from the H_2/Ar experiments for each RF power are shown in Fig. 6(a). Please note the different vertical scales regarding the OES line intensities for different panels in Fig. 6(b). We note that there is an intensity increase for the ArI as well as the HI emission lines with increasing RF power, with a decline in both intensities starting at RF powers of 250 W and beyond. This parallel behaviour of the Ar and H OES lines is in contrast to the corresponding findings from Section 3.1 regarding the O_2/Ar feedstock gas mixture, where the OI line showed a strong increase with RF power whereas the ArI line remained constant. This hints towards different interactions between the various feedstock gases with a corresponding impact onto the cleaning mechanism.

Fig. 7(a) shows the decrease of the carbon layer thickness on both QCM sensors as a function of time and RF power as an additional parameter. As a first significant difference, we note the strongly non-linear behaviour of the cleaning rates shown in Fig. 7(b) with respect to the RF power, which exhibit a saturation starting at about 250 W. Regarding the absolute cleaning values, it is obvious that the cleaning obtained from the H_2/Ar plasma are about a factor of about 6 to 7 lower as compared to the O_2/Ar cleaning rates as has been observed previously [1]. In the present case of the H_2/Ar plasma, we thus also do observe a correlation between the applied RF power and the OES line intensities on one hand as well as the cleaning rates on the other hand, albeit the saturation in both is in sharp contrast to the corresponding linear behaviour in the case of the O_2/Ar plasma.

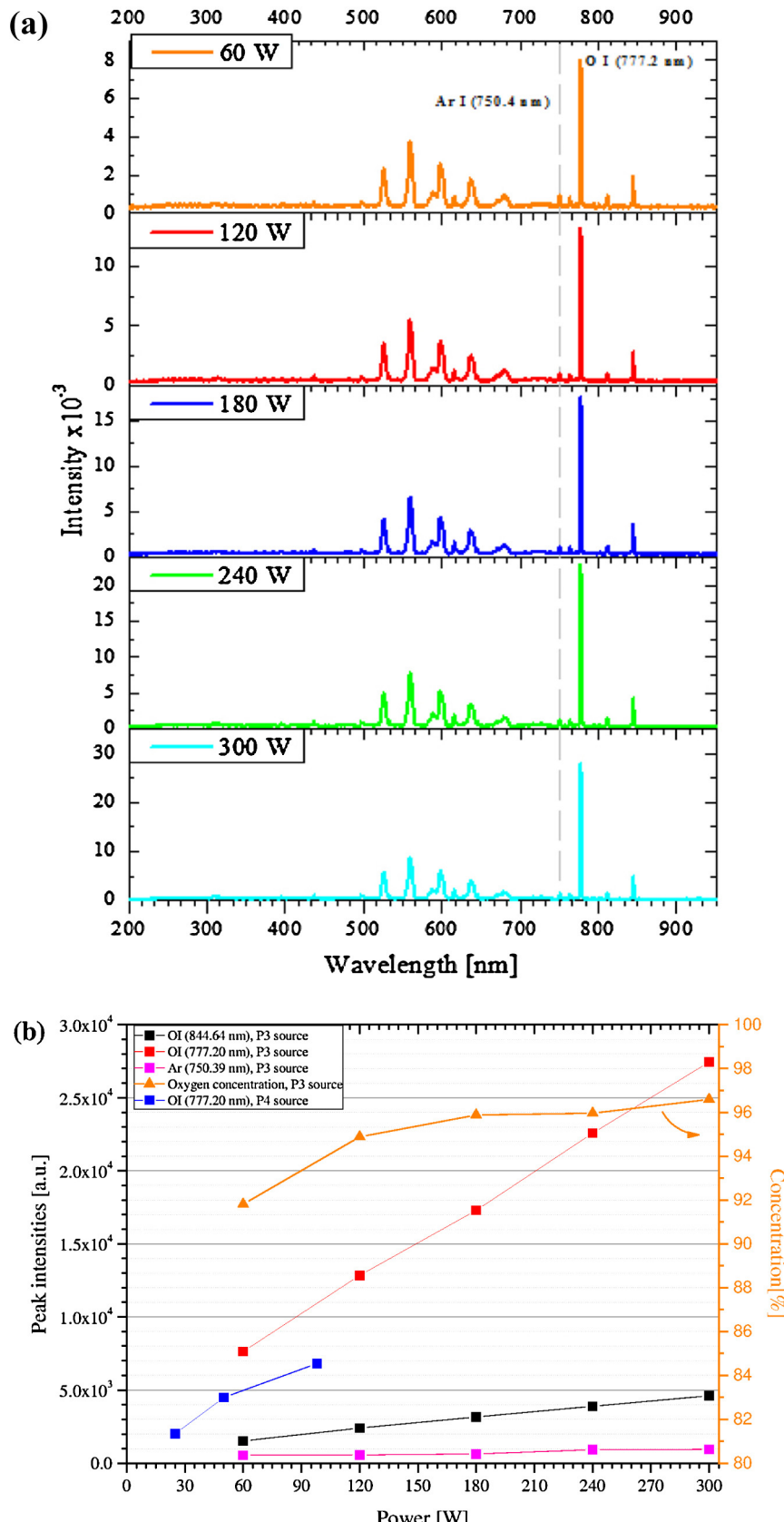


Fig. 4. (a) Optical emission spectra from a typical O_2/Ar cleaning experiment using the P3 source. (b) Intensities of the principal emission lines from the atomic species within the plasma (left hand scale) as well as oxygen concentration (right hand scale) as a function of RF power. "O I" and "Ar I" refer to the left hand side axis (OES peak intensities) meanwhile "Oxygen Concentration" refers to the right hand side axis (Concentration). OES line intensities for OI radicals using the smaller P4 plasma source (blue solid squares) have been added for reference.

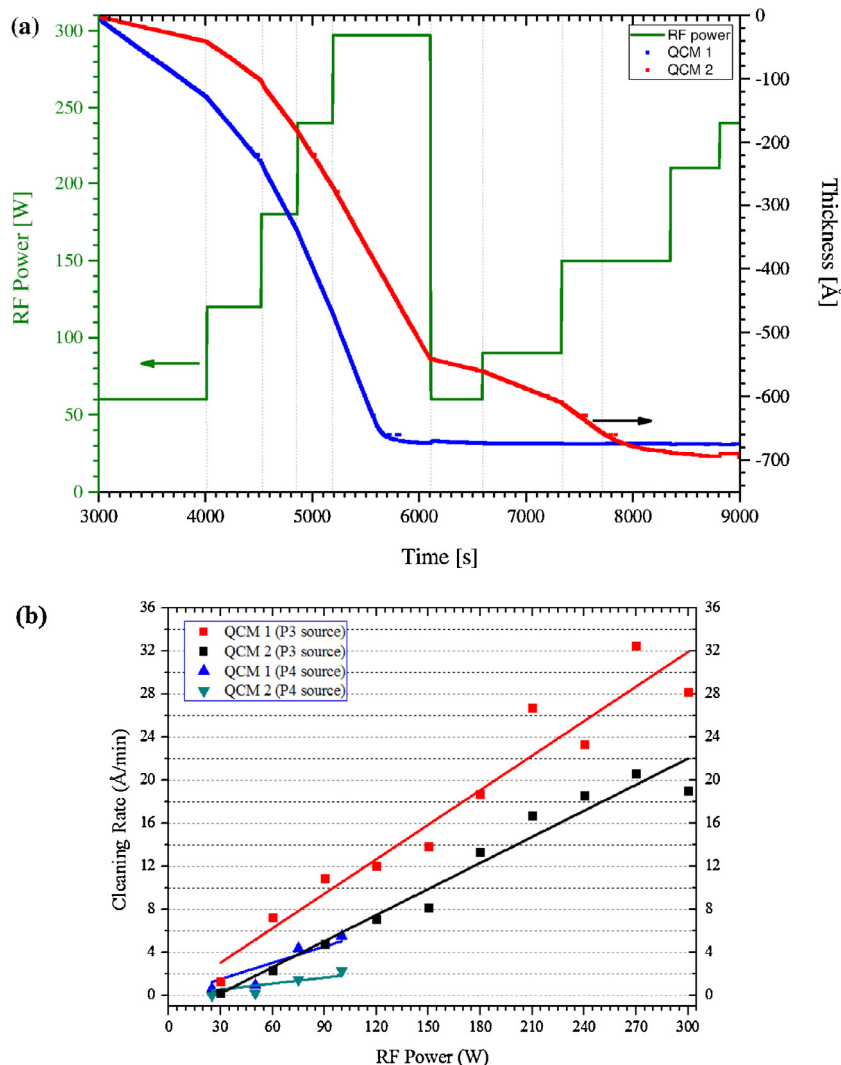


Fig. 5. (a) Measured thickness decrease of the carbon layer on both QCM sensors (red and blue curves) and RF power (green curve) as a function of time. (b) Carbon cleaning rates as a function of RF Power, for the O_2/Ar cleaning of *Amorphous C* samples. Red and black lines/symbols show the cleaning rates for the QCM1 and QCM2 crystals using the larger P3 source, respectively. Blue and green lines/symbols show the cleaning rates for the QCM1 and QCM2 crystals using the smaller P4 source, respectively. The solid lines represent linear fits to the data.

3.3. Comparative cleaning experiments on a diamond-like carbon and amorphous carbon

In this study, the *Amorphous C* samples have been replaced with *DLC* samples by installing them into the QCM1 position (i.e., close to the plasma source). The procedure is the same as in the prior cases, so that the cleaning rates are obtained by determining the temporal derivative of the removed carbon thickness as measured by the QCM quartz crystal balances. Fig. 8 shows the cleaning rate dependence from the RF power (limited to 100 W) for experiments using O_2/Ar or H_2/Ar plasma, respectively.

The cleaning rates for the *DLC* samples are higher for the O_2/Ar case with respect to the values found in the *Amorphous C* samples, meanwhile values for the *DLC* and *Amorphous C* turn out to be comparable when cleaning with H_2/Ar plasma. Hence, we can already anticipate a conclusion: sp^3 -hybridized carbon atoms are more reactive than sp^2 -hybridized carbon atoms with respect to the oxygen radicals within the O_2/Ar plasma.

4. Discussion

After analysing the complete datasets, the results turn out to be consistent with respect to each other: The carbon removal rates

increase with RF power and they decrease when moving away from the plasma source for both O_2/Ar and H_2/Ar plasma. Table 2 gives an overview on the increase in carbon cleaning rates as well as in the corresponding OES line intensities for the RF power range between 60 and 210 W in which all experiments show a linear behaviour as a function of RF power.

As can be seen in Figs. 4(b) and 5(b), for the case of the O_2/Ar plasma cleaning both the OI OES lines intensities as well as the carbon cleaning rate show a linear behaviour for the full RF power range up to 300 W. This result can be expected since the increase of RF power promotes the creation of chemically active species such as, e.g., oxygen radicals within the plasma source that are responsible for the removal of the deposited carbon layer. Interestingly, the QCM1 cleaning rate for the O_2/Ar cleaning shown in Table 2 scales with almost the same factor as the OI OES line intensity (i.e., 3.5 versus 3.7), indicating a one-to-one relationship between the OI radical generation and the carbon removal process.

We differentiate between two different attenuation mechanisms for neutral radicals (i.e., cleaning agents) while traveling within the plasma afterglow along the longitudinal axis of the cylindrical chamber (i.e., emerging from the point-like plasma source and reaching sensor QCM1 first, and then sensor QCM2): diffusion/recombination and geometrical dilution. Non-relativistic

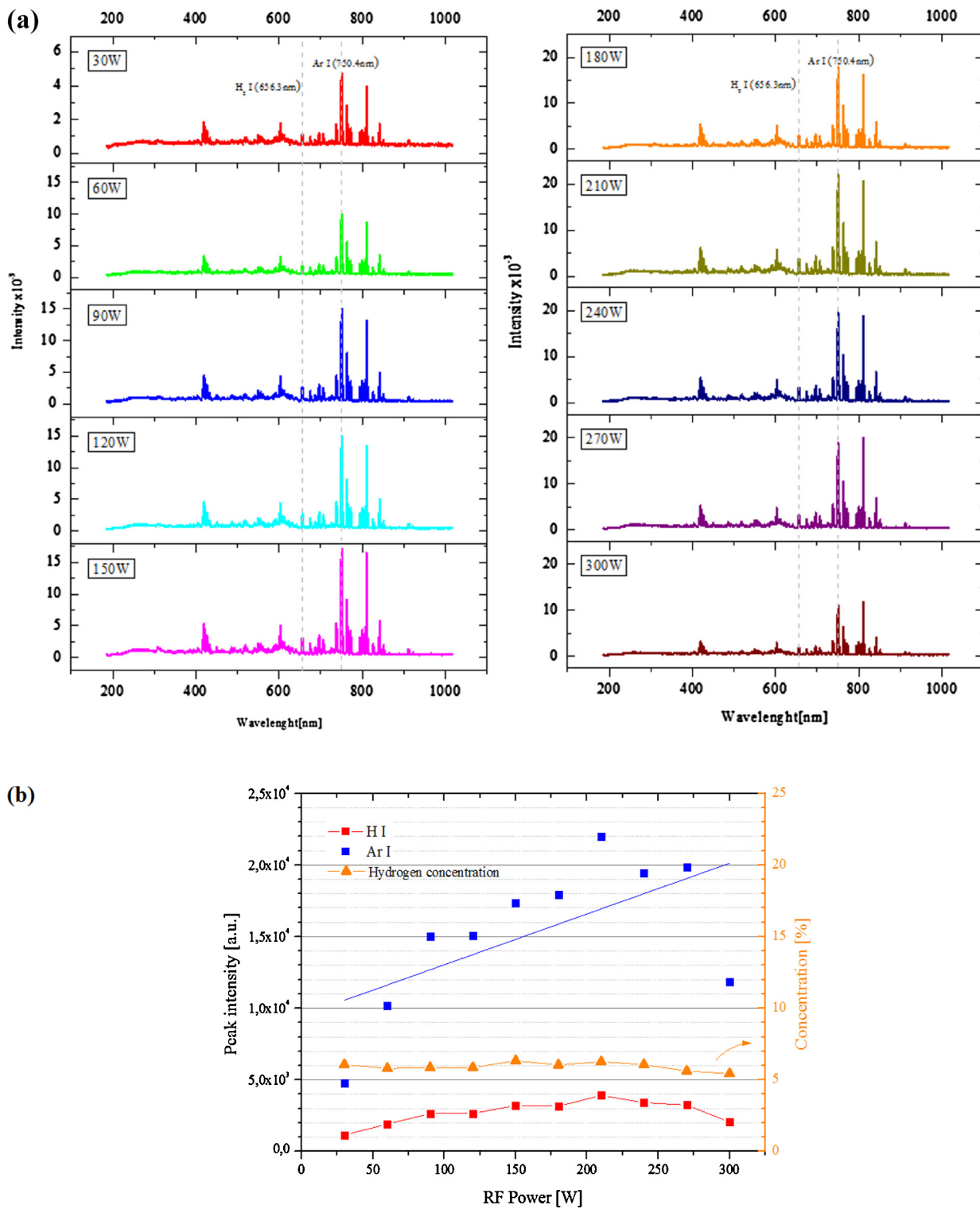


Fig. 6. (a) Optical emission spectra from the H₂/Ar cleaning experiment. (b) Intensities of the principal emission lines from the atomic species within the plasma as a function of RF power. “H I” and “Ar I” refer to the left hand side axis (OES peak intensities) meanwhile “Hydrogen concentration” refers to the right hand side axis (concentration).

particles (such as oxygen and hydrogen radicals in our case) have a finite probability to collide within the downstream plasma afterglow and hence to recombine, thus losing their chemical reactivity for cleaning purposes. This probability depends on the gas temperature and the radical’s “auto-reactivity”. For a given temperature (let us assume radicals with the same thermal energy at room temperature) and density, oxygen radicals will have a smaller

mutual reactivity for recombining into O₂ molecules than hydrogen radicals, thus leading to an enhanced probability for the latter to recombine (i.e., a smaller inelastic mean free path). Diffusion coefficients should therefore be larger for oxygen than for hydrogen radicals. On the other hand, the (purely geometrical) dilution mechanism of radicals – which scales with respect to the distance r from the point source proportional to r^{-3} – is also responsible

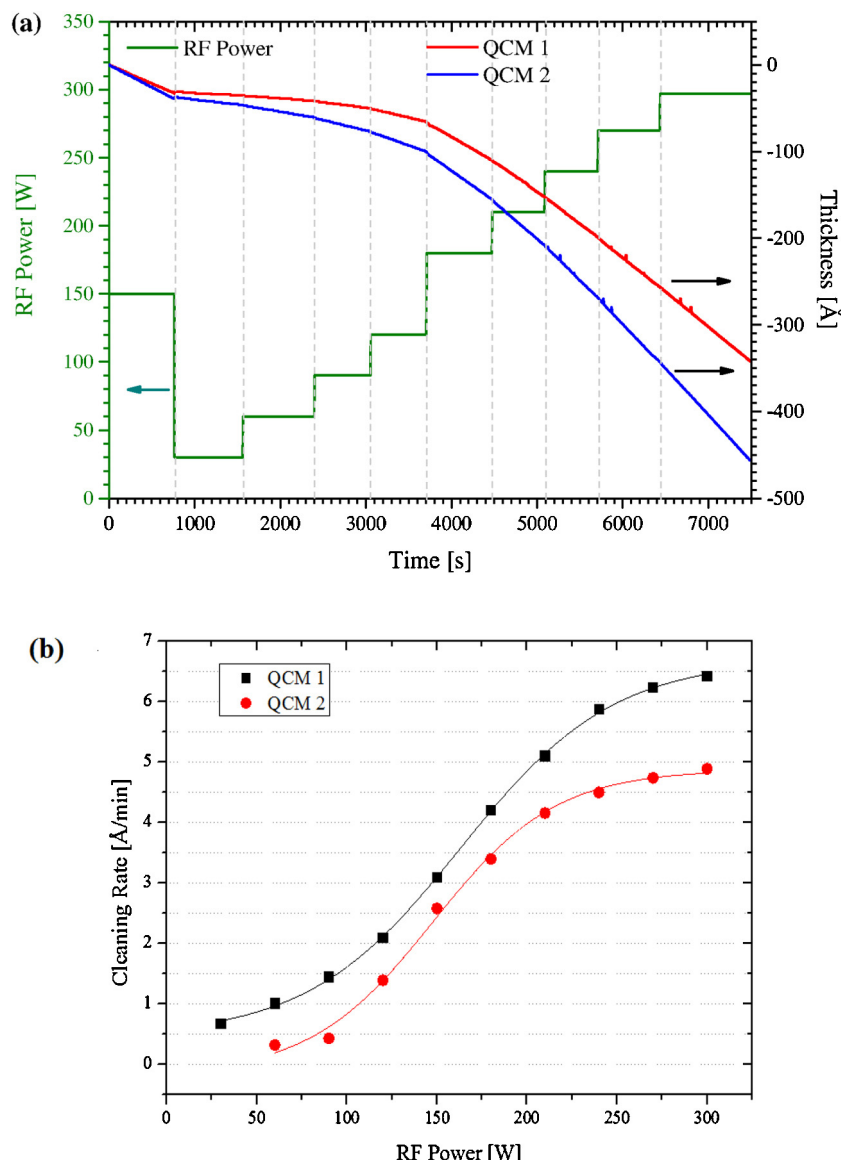


Fig. 7. (a) Measured thickness decrease of the carbon layer on both QCM sensors (red and blue curves) and RF power (green curve) as a function of time. (b) Carbon cleaning rates as a function of RF Power for the H₂/Ar cleaning of the *Amorphous C* samples. The lines serve as guides to the eye.

for the attenuation of the radical density with distance, as the latter spread over a 2π solid angle once the radicals have left the point-like plasma source and propagate within the downstream plasma afterglow along the chamber towards the QCM detectors. This leads to a scaling of the radical flux impinging onto a target unit surface per time unit proportional to r^{-2} , which is the relevant parameter for the carbon cleaning process.

Another important parameter to take into account is the reactivity of the neutral O I and H I radicals with respect to the carbon contaminations, regarding the formation of the gaseous species during the carbon cleaning process. As can be seen from the standard Gibbs free energies of formation in [Table 3](#), the formation of CO₂ and CO are more exothermic as compared than the formation of CH₄ and C₂H₆, thus explaining the constantly larger

Table 2

Increase/decrease factors for the carbon cleaning rates and the corresponding OES line intensities, as measured at 60 and at 120 W RF power (i.e., within the range of linear increase).

	RF Power	QCM1 cleaning rate (Å/min)	QCM2 cleaning rate (Å/min)	Decrease with QCM distance	OI OES line increase at 777.2 nm	ArI OES line increase at 750.4 nm	HI OES line increase at 656.3 nm
O₂/Ar cleaning	120 W	22	16.5	$\times(1.3)^{-1}$			
	60 W	6	3	$\times(2.0)^{-1}$			
	<i>Increase with RF Power</i>	$\times 3.5$	$\times 5.5$		$\times 3.7$	$\times 1.7$	-
H₂/Ar cleaning	120 W	5.7	4.2	$\times(1.3)^{-1}$			
	60 W	1.1	0.3	$\times(3.7)^{-1}$			
	<i>Increase with RF Power</i>	$\times 5.2$	$\times 14$		-	$\times 2$	$\times 1.5$

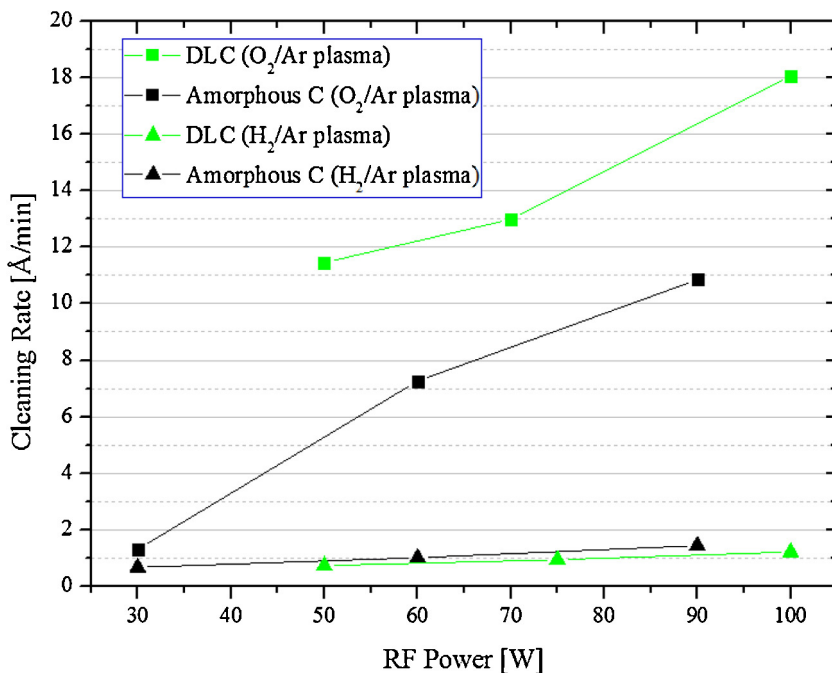


Fig. 8. Comparison between the cleaning rates of *Amorphous C* and *DLC* samples, under O₂/Ar plasma (green and black lines above), and under H₂/Ar plasma (black and green lines below). All of them measured in QCM1.

absolute carbon cleaning rates for O₂/Ar plasma as compared to those from the H₂/Ar plasma.

We first focus on the RF power ranges between 60 and 210 W given in Table 2, where no saturation phenomena do occur in the cleaning rates as a function of RF power.

For the case of the O₂/Ar plasma, cleaning rates decrease with the QCM1 to QCM2 distance by a factor of 1.3 and 2.0 at 120 W and 60 W, respectively, whereas in the case of H₂/Ar we find a reduction factor of 1.3 at 120 W and a surprisingly large factor of 3.7 at 60 W (as shown in Table 2). Assuming that the geometrical dilution mechanism is independent from RF power, this large reduction by a factor of 3.7 speaks in favour of a strong contribution by the diffusion/recombination mechanism. We hypothesize that the low 60 W RF power leads to a low density of radicals, thus allowing for a larger mean free path length and hence making the diffusion mechanism more sensitive to distances within the range of the QCM1 and QCM2 sensors, as the large reduction of factor of 3.7 points out. However, at the conditions of a higher density of radicals right at the source exit (i.e., at 120 W), most of the mutual recombination processes of the hydrogen radicals into H₂ molecules already take place well before reaching sensor QCM1, thus minimizing the diffusion-based differential effect between sensors QCM1 and QCM2 (decrease factor of 1.3). See Fig. 9 for an illustration of these two different scenarios.

This effect is better observed for the H₂/Ar case than in the O₂/Ar case, because of the presumably lower diffusivity for hydrogen than for oxygen radicals. Thus, for both the 120 W and 60 W cases using an O₂/Ar plasma, there is not much appreciable difference with the

RF power variation between QCM1 and QCM2, with similar reduction factors of 1.3 (at 120 W) and 2.0 (at 60 W), respectively. Further measurements of the ions/electrons energy distribution with, e.g., a Faraday cup at different distances and powers, would help to corroborate this hypothesis and get a more quantitative picture for Fig. 9.

Focusing now on the increase of cleaning rates with RF power, one can see in Table 2 that for the case of H₂/Ar plasma, the pertinent factors are 5.2 and 14 for the QCM1 and QCM2 sensors, respectively. Besides an increase of HI radical density at larger RF power, the larger increase in cleaning rate for the case of the more distant QCM2 sensor – together with the much smaller increase for the HI OES line (factor of 1.5) – indicates a combined/cooperative effect between the hydrogen radicals and the increase of UV light generated by the Ar species. This additional contribution to the carbon removal rate by the generation of UV light is already known from the photon-assisted breaking of carbon bonds and the subsequent reduction of carbon in plasma applications related to the production of hydrocarbon gas from coal (see, e.g., Ref. [16]).

On the other hand and as already mentioned above, the increase by a factor of 3.5 and 5.5 for the QCM1 and QCM2 sensors for the O₂/Ar plasma as a function of RF power together with a similarly strong increase of the OI OES line by a factor of 3.7 yields the one-to-one relationship between the density of OI radicals and cleaning rates mentioned previously. The larger increase for the more distant QCM2 indicates an additional contribution by the inelastic mean free path length of the OI radicals at source-QCM2 distances. All this demonstrates that in the specific case of O₂/Ar feedstock gases, the application of larger RF powers are beneficiary for larger optical components to be cleaned due to (i) a higher density of reactive OI radicals and (ii) a less effective inelastic mean free path length at larger source-object distances by dilution.

In order to put the above results into a more quantitative context (as we are severely limited regarding the availability of standard plasma diagnostics), we give some pertinent gaseous diffusion coefficients from the literature. For the room temperature diffusion coefficients of O in O₂ and O in Ar at 300 K, we find 205 and 296 Torr cm² s⁻¹, respectively, which – taking into account the

Table 3

Standard Gibbs free energy of formation for various gaseous products from the carbon cleaning using oxygen and hydrogen radicals [15].

Active species	Molecule	Standard Gibbs free energy of formation ΔG_f° at 300 K [kJ/mol]
OI(O [•])	CO	-137.23
	CO ₂	-394.4
HI(H [•])	CH ₄	-50.8
	C ₂ H ₆	-32.9

Table 4

Gas diffusion coefficients and mean square displacements for O and H radicals in different carrier gas mixtures and temperatures as reported in the literature.

Radical	Carrier gas	Gas temperature [K]	Diffusion coefficient [$\text{Torr cm}^2 \text{s}^{-1}$]	Mean square displacement [cm^2]	References
O I	O ₂	300	205	27.4	Yolles and Wise [17]
O I	Ar	300	296	39.5	Yolles and Wise [17]
H I	13% H ₂ and 87% Ar	343	876	117	Wise [18]
H I	H ₂	343	1386	182	Sanier and Wise [19]
H I	H ₂	498	115	15.3	Grubbs and George [20]

pressure of 0.005 mbar during our experiments as well as an estimated typical collision rate in the range of 2 kHz – result into a mean square displacement of 27.4 and 39.5 cm^2 [17]. Other pertinent diffusion coefficients are given in Table 4. The numbers clearly show that the mean square displacements are well within the relevant engineering dimensions regarding the distances between the GV10x source and the QCM1 and QCM2 sensors, which tells us that diffusion phenomena should be taken into account in our experiments.

As can be seen from Table 4, the O (in O₂) and H (in 13% H₂/87% Ar—which is the close to our H₂/Ar feedstock gas mixture) diffusion coefficients close to room temperature exhibit a trend that is in opposite to our above findings that did indicate a larger diffusion coefficient for O (in O₂) than for H (in H₂/Ar). However, taking a comparative look at the evolution of the diffusion coefficients for H (in H₂) with temperature, it is obvious that a temperature increase from 343 to 498 K can easily result into a reduction of the diffusion coefficient and the associated mean square displacement by a factor of more than ten. We would thus like to assign this discrepancy to the – so far unknown – gas temperatures close to the GV10x exhaust as well as in the downstream cleaning chamber volume. Taking into account the experimental observation of a strong temperature increase of the vacuum tubes just downstream the source exhaust due to the exothermic recombination of the HI radicals specifically for the H₂/Ar plasma (see below), this pinpoints a noteworthy difference between the two plasma we have been using. Moreover, this difference in terms of gas temperature could explain the above discrepancy regarding the magnitude of the OI and HI diffusion coefficients.

We now discuss the power dependence of the cleaning rates in Fig. 5(b) and 7(b) up to the maximum RF power of 300 W. In contrast to the linear increase of the O₂/Ar cleaning rates with power as discussed above, the behaviour of the cleaning rates in the case of the H₂/Ar plasma is completely different: At lower RF power the cleaning rates grow exponentially, but at higher RF power (i.e., at 250 W and beyond), there is a distinct saturation of the carbon removal rate. Also, as can be seen from Fig. 6(b) and Table 2, the number of HI radicals (as given by the intensity of the HI OES line)

as well as the Ar I OES line show a rather weak linear increase by a factor of about 1.5 and 2, respectively, up to about 210 W RF power. This is in contrast to the large increase in QCM1 and QCM2 cleaning rates by a factor of 5.2 and 14, respectively. Again, the larger increase in cleaning rate – as compared to the smaller increase for the OES lines – could indicate a combined/cooperative effect of the hydrogen radicals and the increase of UV light generated by the Ar for the carbon removal.

Regarding the saturation in terms of cleaning rate for the specific case of the H₂/Ar plasma at high RF power (see Fig. 7(b)), we assume that this is not caused by a passivation of the sample surface by the plasma, as we do not observe this type of saturation effect for the O₂/Ar case. As discussed in Ref. [1], we rather attribute this saturation to the recombination of hydrogen HI radicals into H₂ molecules by their mutual interaction and/or via the interaction with the 304L stainless steel vacuum recipient walls as has already been discussed by several authors [20,21]. This effect appears to be much more intense in the case of the hydrogen radicals as they have a higher reactivity than the oxygen OI radicals. Hence, the cleaning experiments using H₂/Ar suffer from saturation in the density of HI radicals available for the cleaning process, which explains the saturation at high RF powers in Fig. 7(b). Indeed, we measured unusually elevated temperatures around 70 °C on the metal vacuum tubes downstream the plasma source, when operating it with H₂/Ar at high RF powers for a longer period of time. This effect occurs presumably due to the exothermic recombination of hydrogen radicals into molecules on the in-vacuum metal surfaces. All this fits well into the overall conceptual approach that hydrogen plasma need either to be embedded into an inert carrier gas matrix (such as, e.g., Ar) or to be provided with lower HI radical densities in order to allow for the mean free path lengths required for any large scale cleaning application. A direct measurement of the HI radical density at the QCM sensor is needed in order to corroborate the hypothesis of HI radical loss due to recombination.

We now discuss the carbon cleaning efficiency for the two different carbon allotropes under investigation (see Fig. 8). The differences between the cleaning rates for *Amorphous C* and *DLC* samples were studied separately for the case of O₂/Ar and H₂/Ar

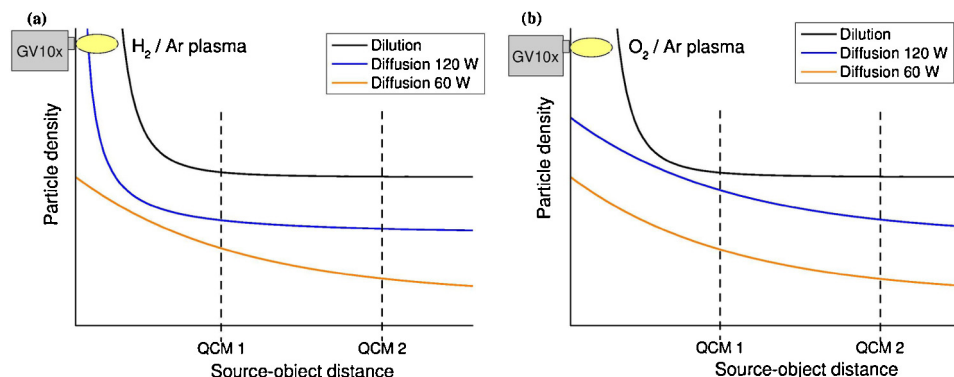


Fig. 9. Qualitative comparison between the dilution and diffusion mechanisms at 60 W and 120 W, for the case of (a) H₂/Ar and (b) O₂/Ar plasma. For the H₂/Ar plasma, even though the absolute number of charged ions is larger at 120 W, the diffusion rate has already reached a “flat” region when passing by the QCM sensors, so that the cleaning rates are not as power-dependent as for the 60 W low RF power case. This does not apply to the O₂/Ar case.

plasma. The sp^3 carbon (*DLC* samples) turned out to exhibit cleaning rates about 1.4 times higher than the amorphous samples (*Amorphous C*) under O_2/Ar plasma, which speaks in favour of an enhanced reactivity of the sp^3 -bonded carbon atoms as compared to sp^2 carbon with respect to oxygen radicals. On the other hand, there is no evidence for a significant change in cleaning speed for the two different allotropes in the case of a H_2/Ar plasma. Although the difference in cleaning speeds between *Amorphous C* and *DLC* for an O_2/Ar plasma is significant, we conclude that this latter feedstock gas combination is an appropriate choice for an efficient cleaning of both carbon allotropes, thus covering most optics cleaning applications. As mentioned in Ref. [1], albeit the strongly reduced cleaning rates of H_2/Ar plasma, it is the method of choice for non-noble metal optical coatings that would be subject to oxidation by an O_2/Ar cleaning process.

Several early as well as more recent studies [22–24] aimed at the deposition of graphene nano-sheets, single-crystalline graphene, diamond or their nano-crystalline counterparts have emphasized the importance of adding low quantities of either oxygen or hydrogen to the main feedstock gases such as, e.g., methane or diethylene where the latter are used as carbon sources for the thin film deposition process. In this context, the mentioned hydrogen or oxygen add-on gases are then used as cleaning agents for avoiding the nucleation of undesirable sp^2 or sp^3 carbon intergrowths, depending on the specific type of carbon allotrope to be grown.

5. Conclusions

We have performed a comparative study regarding the low-pressure (i.e., 5×10^{-3} mbar) RF plasma cleaning rates for O_2/Ar and H_2/Ar feedstock gases throughout a wide range of RF powers and source-sample distances which are parameters being relevant for and compatible with applications in the field of cleaning of optical precision surfaces of real-size optics from carbon contaminations made of virtually different carbon allotropes. From this study, we derive the following conclusions:

- Satisfactory cleaning rates well beyond 10 \AA min^{-1} can be obtained in the case of reasonably large optics chambers (i.e., of 1 m length or more) using O_2/Ar feedstock gases with RF powers just beyond 150 W.
- The above holds for both amorphous carbon (i.e., sp^2 and sp^3 mixtures) and especially diamond-like carbon sp^3 allotropes.
- The carbon cleaning rates for O_2/Ar feedstock gas as well as the density of OI (or O[·]) neutral oxygen radicals scale linearly with increasing RF power. The increase in cleaning rate as a function of RF power increases with increasing source-object distance, thus indicating the influence of a less effective OI inelastic mean free path length for larger source-object distances.
- The carbon cleaning rates for H_2/Ar feedstock gas exhibits a strongly “S-shaped” sigmoidal behaviour with increasing RF power saturating at higher powers, whereas the density of HI neutral radicals shows a (weak) linear increase with RF power. From this, we conclude a combined/cooperative effect between the HI (or H[·]) radicals and the UV light generated by the Ar atomic species regarding the carbon cleaning rates.
- For H_2/Ar plasma, the increase in cleaning rate as a function of RF power increases with increasing source-object distance (up to intermediate RF power), again indicating the influence of a less

effective inelastic mean free path length for increasing source-object distances also for HI (or H[·]) radicals.

- At elevated RF powers and thus higher HI (or H[·]) radical densities, the high reactivity of the hydrogen radicals leads to an increase in recombination to chemically inactive H_2 molecules and thus to a saturation in cleaning rate.

Acknowledgements

The authors would like to acknowledge the help by Guillaume Sauthier (ICN2) for his collaboration during the XPS characterization. We also thank ibss Group Inc. for supplying the GV10x DS Asher systems as well as the *DLC* samples.

References

- [1] E. Pellegrin, I. Šics, J. Reyes-Herrera, C. Pérez Sempere, J.J. Lopez Alcolea, M. Langlois, J. Fernandez Rodriguez, V. Carlino, Characterization, optimization and surface physics aspects of in situ plasma mirror cleaning, *J. Synchrotron Radiat.* 21 (2014) 300–314.
- [2] S. Graham, C. Steinhäus, M. Clift, L. Klebanoff, Radio-frequency discharge cleaning of silicon-capped Mo/Si multilayer extreme ultraviolet optics, *J. Vac. Sci. Technol. B* 20 (2002) 2393.
- [3] A. Thedsakulwong, W. Thowladda, Removal of carbon contamination on silicon wafer surfaces by microwave oxygen plasma, *J. Metals Mater. Miner.* 18 (2008) 137–141.
- [4] E. Strein, D. Allred, M.R. Linford, Use of a commercial RF plasma cleaner in eliminating adventitious carbon contamination in an XPS system, *Microsc. Microanal.* 14 (2008) 818–819.
- [5] T.C. Isabell, P.E. Fischione, C. O'Keefe, M.U. Guruz, V.P. Dravid, Plasma cleaning and its applications for electron microscopy, *Microsc. Microanal.* 5 (1999) 126–135.
- [6] F. Eggenstein, F. Senf, T. Zeschke, W. Gudat, Cleaning of contaminated XUV-optics at BESSY II, *Nucl. Instrum. Methods Phys. Res. A* 325 (2001) 467–468.
- [7] E.D. Johnson, R.F. Garrett, In situ glow discharge cleaning of x-ray optical surfaces, *Nucl. Instrum. Methods Phys. Res. A* 266 (1988) 381.
- [8] J. Diaz, G. Paolicelli, S. Ferrer, F. Comin, Separation of the sp^3 and sp^2 components in the C1s photoemission spectra of amorphous carbon films, *Phys. Rev. B* 54 (1996) 8064.
- [9] P. Méril, M. Tabbal, M. Chaker, S. Mosa, J. Margot, Direct evaluation of the sp^3 content in diamond-like carbon films by XPS, *Appl. Surf. Sci.* 136 (2010) 105–110.
- [10] A.C. Ferrari, D.M. Basko, Raman spectroscopy as a versatile tool for studying the properties of graphene, *Nat. Nanotechnol.* 8 (2013) 235.
- [11] A.C. Ferrari, J.C. Meyer, V. Scardaci, C. Casiraghi, M. Lazzeri, F. Mauri, S. Pisacane, K.S. Da Jiang, S. Novoselov, A.K. Roth, Geim, The Raman fingerprint of graphene, *Phys. Rev. Lett.* 97 (2006) 187401.
- [12] J. Schwan, S. Ulrich, V. Batori, H. Ehrhardt, S.R.P. Silva, Raman spectroscopy on amorphous carbon films, *J. Appl. Phys.* 80 (1996) 440–447.
- [13] P.W. May, J.A. Smith, K.N. Rosser, 785 nm Raman spectroscopy of CVD diamond films, *Diam. Relat. Mater.* 17 (2008) 199–203.
- [14] A. Kramida, Yu.Ralchenko, J. Reader, NIST ASD Team, NIST Atomic Spectra Database (ver. 5.1), 2013.
- [15] Dean, A. John (Eds.), *Lange's Handbook of Chemistry*, 15th ed., McGraw-Hill, New York, 1999.
- [16] A. Fridman, *Plasma Chemistry*, Cambridge University Press, New York, 2008.
- [17] R.S. Yolles, H. Wise, Diffusion and heterogeneous reaction X. Diffusion coefficient measurements of atomic oxygen through various gases, *J. Chem. Phys.* 48 (1968) 5109.
- [18] H. Wise, Diffusion coefficient of atomic hydrogen through multicomponent mixtures, *J. Chem. Phys.* 31 (1959) 1414.
- [19] K.M. Sanier, H. Wise, Diffusion and heterogeneous reaction XI. Diffusion coefficient measurements for gas mixture of atomic and molecular hydrogen, *J. Chem. Phys.* 51 (1969) 1434.
- [20] R.K. Grubbs, S.M. George, Attenuation of hydrogen radicals traveling under flowing gas conditions through tubes of different materials, *J. Vac. Sci. Technol. A* 24 (2006) 486.
- [21] W.V. Smith, The surface recombination of H atoms and OH radicals, *J. Chem. Phys.* 11 (1943) 110.
- [22] L. Zhang, Z. Shi, D. Liu, R. Yang, D. Shi, G. Zhang, Vapour-phase graphene epitaxy at low temperatures, *Nano Res.* 5 (2012) 258.
- [23] G. Nandamuri, S. Roumimov, R. Solanki, Remote plasma assisted growth of graphene films, *App. Phys. Lett.* 96 (2010) 154101.
- [24] S. Vizireanu, B. Mitu, C.R. Luculescu, L.C. Nistor, G. Dinescu, PECVD synthesis of 2D nanostructured carbon material, *Surf. Coat. Technol.* 211 (2012) 2.